

Numerical Simulation and Performance Evaluation of Highly Efficient Sb_2Se_3 Solar Cell with Tin Sulfide as Hole Transport Layer

Adil Sunny and Sheikh Rashel Al Ahmed*

This work reports a numerical investigation on the performance of Sb_2Se_3 -based thin-film heterojunction solar cell using the solar cell capacitance simulator in 1D (SCAPS-1D) program. Herein, inorganic tin sulfide (SnS) is introduced as a new hole transport material into the Sb_2Se_3 solar cell. The effects of several parameters such as thickness, doping, electron affinity, defect density, temperature, and resistances on the cell performances are analyzed. The proposed novel solar configuration that consists of Al/F:SnO₂ (FTO)/CdS/ Sb_2Se_3 /SnS/Mo reveals the enhanced photovoltaic performances by means of reducing carrier recombination loss at back surface. At an optimized Sb_2Se_3 thickness of 1.0 μm , the efficiency is boosted from 24.01% to 29.89% by incorporating an ultrathin 0.05 μm SnS hole transport layer (HTL) into the Sb_2Se_3 solar cell. The performances of the proposed device are also evaluated by varying defects at CdS/ Sb_2Se_3 and Sb_2Se_3 /SnS interfaces. Moreover, it is found that electron affinity larger than 3.5 eV of HTL as well as back contact metal work function ≥ 4.9 eV should be considered to attain better performance. The simulated results lead to suggest that introducing the SnS material as a potential HTL candidate would be useful to develop low-cost and highly efficient thin-film solar cells.

1. Introduction

Thin-film solar cells (TFSCs) based on semiconductors have been attracting great consideration for photovoltaic device application owing to their pollution-free system, low cost, ease of fabrication, excellent optoelectronic properties, and highly efficient power conversion.^[1–14] However, further enhancement in conversion efficiency of the TFSCs has been limited due to low elemental abundance, expensive, and high toxicity of materials. Although several prominent studies have been investigated to explore alternative nontoxic, earth-abundant, and cost-effective absorber materials in the TFSCs to overcome the limitations,^[15–19] no previous attempts have been successful to achieve satisfactory conversion efficiency by the materials.

In the last few years, antimony selenide (Sb_2Se_3) semiconductor has received considerable attention as an attractive absorber material in the thin-film heterojunction photovoltaic device due to its high absorption coefficient ($>10^5 \text{ cm}^{-1}$), favorable energy bandgap (1–1.2 eV), reasonable carrier mobility, low toxicity, earth-abundant constituents, inexpensive, low temperature fabrication process, and excellent stability.^[20–30] In the previous works, several experimental^[20–23, 27, 31–40] and theoretical^[41–47] studies on improving the performances of the Sb_2Se_3 -based solar cells have been reported. There have been numerous experimental Sb_2Se_3 -based heterojunction solar structures, including $\text{TiO}_2/\text{Sb}_2\text{Se}_3$,^[18] $\text{TiO}_2/\text{Sb}_2\text{Se}_3/\text{CuSCN}$,^[31] $\text{CdS}/\text{Sb}_2\text{Se}_3$,^[23, 32, 33, 35, 36, 38–40] $\text{CdS}/\text{Sb}_2\text{Se}_3/\text{PbS}$,^[34] and $\text{CdS}/\text{Sb}_2\text{Se}_3/\text{CuSCN}$,^[37] described to achieve excellent photovoltaic performance. The more recent experimental efficiency of the Sb_2Se_3 solar cell has been reported to be 9.2% with a device structure of $\text{ZnO:Al}/\text{ZnO}/\text{CdS}/\text{TiO}_2/\text{Sb}_2\text{Se}_3$ nanorod arrays/ MoSe_2/Mo .^[27] On the other hand, the numerical simulation approaches on the Sb_2Se_3 solar cells with different heterostructures of CdS/ Sb_2Se_3 ,^[41] ZnO/CdS/ Sb_2Se_3 ,^[42] hole transport layer (HTL)/ Sb_2Se_3 /electron transport layer (ETL),^[43] $\text{In}_2\text{S}_3/\text{Sb}_2\text{Se}_3/\text{Cu}_2\text{O}$,^[44] CdS/ Sb_2Se_3 /HTL,^[45] $\text{Zn}_{0.93}\text{Mg}_{0.07}\text{O}/\text{ZnO}_{0.4}\text{S}_{0.6}/\text{TiO}_2/\text{Sb}_2\text{Se}_3/\text{MoSe}_2$,^[46] and $\text{Zn}(\text{Sn},\text{O})/\text{Sb}_2\text{Se}_3/\text{CZTSe}$ ^[47] report the conversion efficiency to lie in the range of 11.52–24.7%. However, the obtained efficiencies with the previous different device configurations for the Sb_2Se_3 solar cell are still lower than the commercially available TFSCs as well as from the expected Shockley–Queisser efficiency limit of 32.23%.^[11, 12, 48, 49] Very recently, 0.3 μm -thick barium silicide as a back surface field layer at the back of Sb_2Se_3 absorber material is incorporated in the Sb_2Se_3 -based TFSC to achieve the highest conversion efficiency numerically.^[50]

The limited photovoltaic performance may be causes of the basic factors such as carrier recombination at back surface and inefficient carrier transportation and collection by the back and front contacts. Therefore, to achieve optimum photovoltaic outputs, further study on designing of a new Sb_2Se_3 -based TFSC is needed. This device modeling guideline would be useful for the designer and researcher to develop a high-efficiency solar cell practically. It has been demonstrated that the hole transport from the absorber to back contact with low carrier recombination rate can be significantly enhanced by adding HTL between the

A. Sunny, Dr. S. R. A. Ahmed
 Department of Electrical, Electronic and Communication Engineering
 Pabna University of Science and Technology
 Pabna 6600, Bangladesh
 E-mail: rashel@pust.ac.bd

 The ORCID identification number(s) for the author(s) of this article can be found under <https://doi.org/10.1002/pssb.202000630>.

DOI: 10.1002/pssb.202000630

absorber and the back metal contact.^[43,51,52] In the previous studies, the inorganic tin sulfide (SnS) as a HTL has been applied to improve the performances of the photovoltaic devices.^[53–55] Several advantages, such as nontoxicity, earth-abundant, suitable energy bandgap, high absorption coefficient, high carrier mobility, and low cost, make the SnS as a promising candidate for the HTL in the thin-film heterojunction solar cells.^[56–59] In the present work, the SnS as the HTL is proposed to the basic Sb₂Se₃-based heterojunction TFSC.

In this article, the modeling and numerical simulation of the Sb₂Se₃-based TFSC with a novel heterostructure of Al/F:SnO₂ (FTO)/CdS/Sb₂Se₃/SnS/Mo have been presented, where the CdS and SnS have been used as the ETL and HTL, respectively. A comparative analysis on the performance evaluation of the Sb₂Se₃ solar cells without and with HTL is also demonstrated. The solar cell capacitance simulator in 1D (SCAPS-1D) simulation software has been utilized to investigate the photovoltaic performance of the proposed novel device structure by varying different physical parameters of the absorber, ETL, and HTL.

2. Device Simulation and Materials Properties

In the present work, the 1D solar cell device simulator, namely, SCAPS-1D program developed by the University of Gent,^[60] has been carried out to model and simulate the TFSC based on Sb₂Se₃ absorber. The SCAPS-1D simulation tool is capable of solving three basic equations of semiconductor devices, such as Poisson's equation, the carrier continuity equation, and the drift-diffusion equation.^[60–63] The current-voltage (*I*-*V*), capacitance-voltage (*C*-*V*), capacitance-frequency (*C*-*f*) characteristics, external quantum efficiency (EQE), and recombination profile of the photovoltaic devices can be analyzed using the SCAPS-1D simulator. In this numerical approach, the influences of the thickness, doping concentration, electron affinity, bulk defect density in absorber, interface defect density, operating temperature and metal work function, and resistances on the performance of Sb₂Se₃-based solar cell have also been investigated. All the simulation has been conducted under an

illumination of 100 mW cm⁻² and AM1.5 G light spectrum at an operating temperature of 300 K. Figure 1a demonstrates the schematic diagram of the Al/FTO/CdS/Sb₂Se₃/SnS/Mo heterojunction device architecture. The energy level diagram of the proposed TFSC structure is also shown in Figure 1b. An ultra-thin p⁺-type SnS HTL is inserted between the p-type Sb₂Se₃ absorber and the back metal contact. In the proposed device configuration, the n-type CdS as an ETL and fluorine-doped tin oxide (F:SnO₂) as a transparent conducting oxide (TCO) layer are also used, respectively. Aluminum (Al) and molybdenum (Mo) with the work functions of 4.06 eV and 4.95 eV are utilized as the front and back metal contacts in the TFSCs, respectively.^[64] Table 1 represents the required physical parameters of different layers for this simulation work. The values of the material parameters

Table 1. Simulation parameters used in the proposed Sb₂Se₃ TFSC with SnS HTL.

Parameters [unit] ^{a)}	TCO (F:SnO ₂)	ETL (CdS)	Absorber (Sb ₂ Se ₃)	HTL (SnS)
Thickness [μm]	0.05	0.05 ^{b)}	1.0 ^{b)}	0.05 ^{b)}
E _g [eV]	3.6 ^[69]	2.4 ^[65]	1.06 ^[20]	1.10 ^[59]
χ [eV]	4 ^[69]	4.2 ^[66,67]	3.90 ^[20]	3.52 ^[59]
ε _r	9 ^[69]	10 ^[65]	18 ^[25]	12.50 ^[59]
N _C (cm ⁻³)	2.2 × 10 ¹⁸ ^[69]	2.2 × 10 ¹⁸ ^[65]	2.2 × 10 ¹⁸ ^[41,45]	7.5 × 10 ¹⁸ ^[59]
N _V (cm ⁻³)	1.8 × 10 ¹⁹ ^[69]	1.8 × 10 ¹⁹ ^[67]	1.8 × 10 ¹⁹ ^[41,45]	1.0 × 10 ¹⁹ ^[59]
μ _e (cm ² V s ⁻¹)	100 ^[69]	100 ^[65,67]	15 ^[68]	100 ^[59]
μ _h (cm ² V s ⁻¹)	25 ^[69]	25 ^[65,67]	5.1 ^[20]	4 ^[59]
N _D (cm ⁻³)	1 × 10 ¹⁸	1 × 10 ^{17b)}	0	0
N _A (cm ⁻³)	0	0	1 × 10 ^{17b)}	1 × 10 ^{19b)}
Defect-type	–	SA	SD	SD
N _t (cm ⁻³)	–	1 × 10 ¹⁵	6.9 × 10 ^{14b)} ^[25,50]	1 × 10 ¹⁵

^{a)} E_g: energy bandgap; χ: electron affinity; ε_r: relative permittivity; N_C: conduction band density of states; N_V: valance band density of states; μ_e: electron mobility; μ_h: hole mobility; N_D: donor concentration; N_A: acceptor concentration; SA = single acceptor; SD = single donor; and N_t: Defect density; ^{b)} Variable field.

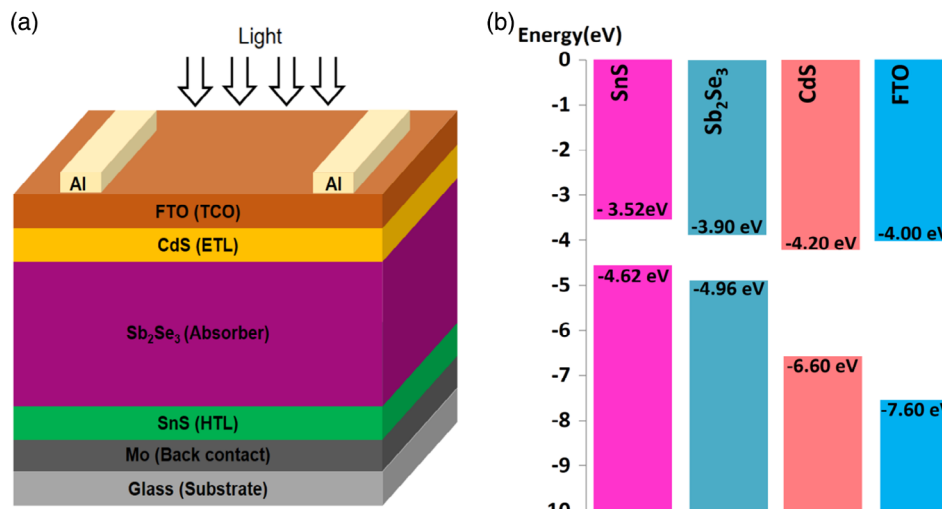


Figure 1. a) Schematic and b) energy level diagrams of the proposed Sb₂Se₃-based solar cell structure.

Table 2. Defect parameters at the CdS/Sb₂Se₃ and Sb₂Se₃/SnS interfaces.

Parameters (unit)	CdS/Sb ₂ Se ₃ interface	Sb ₂ Se ₃ /SnS interface
Defect-type	Neutral	Neutral
Capture cross section of electrons (cm ²)	1×10^{-19}	1×10^{-19}
Capture cross section of holes (cm ²)	1×10^{-19}	1×10^{-19}
Reference for defect energy level E _t	above the highest E _v	above the highest E _v
Energy with respect to reference (eV)	0.01	0.01
Total density (cm ⁻²)	1×10^{10}	1×10^{10}

for the numerical calculations are adopted from the literature.^[20,22,41,45,50,59,60,65–69] The thermal velocities of electrons and holes are assumed to be $\approx 1 \times 10^7$ cm s⁻¹.^[50,70] The values of absorption coefficient allocated for the Sb₂Se₃ absorber and the SnS HTL materials are taken from the literature,^[20,71] whereas the absorption coefficient values of CdS and SnO₂ are selected from SCAPS-1D software.^[60] The single-type defect with Gaussian energetic distribution is chosen. The energy levels of the defect are set to the center of the bandgap. For simplicity of calculation, trap capture cross sections and surface recombination velocity for both electrons and holes are kept fixed at 1×10^{-15} cm² and 1×10^7 cm s⁻¹, respectively. In this numerical study, the defect density at both the ETL/absorber and the absorber/HTL is introduced to understand the interface carrier recombination in the heterojunction TFSC. The parameters of the interface defects are shown in **Table 2**.

3. Results and Discussion

3.1. Device Performances of Sb₂Se₃ Solar Cells without and with HTL

The device performances of the Sb₂Se₃-based thin-film heterojunction solar structures of Al/FTO/CdS/Sb₂Se₃/Mo (without HTL) and Al/FTO/CdS/Sb₂Se₃/SnS/Mo (with HTL) are evaluated using the SCAPS-1D simulation software at a temperature of 300 K, as shown in **Figure 2**. The simulated J-V characteristics, energy band diagram, electric field distribution at the absorber/HTL interface, and EQE as a function of the wavelength of the Sb₂Se₃-based TFSCs are represented in Figure 2a-d. To realize device performances, the thicknesses of 0.05, 0.05, 1.0, and 0.05 μm have been used initially for the TCO, ETL, absorber, and HTL, respectively.

Figure 2a shows the influence of HTL on the photovoltaic performances based on the J-V characteristics. The simulation results show that the calculated performance parameters such as open-circuit voltage (V_{oc}), short-circuit current density (J_{sc}), fill-factor (FF), and efficiency of the Sb₂Se₃-based TFSC without HTL are low of 0.662 V, 45.44 mA cm⁻², 79.88%, and 24.01%, respectively. These results are in good agreement with the results reported in the literature.^[50] On the other hand, the solar cell introducing SnS HTL enhances the output parameters significantly. The values of V_{oc} , J_{sc} , FF, and efficiency of the proposed Sb₂Se₃-based TFSC are estimated to be 0.705 V, 51.40 mA cm⁻², 82.50%, and 29.89%, respectively. The calculated high J_{sc} of the

proposed solar cell with SnS HTL may be attributed to a high absorption coefficient of the material. The high absorption coefficient causes absorption depth to be very low, which ultimately creates more photogenerated charge carriers and, thus, increases J_{sc} greatly. In the previous works, the short-circuit current density larger than 50 mA cm⁻² has been reported for the thin-film heterojunction solar cells.^[50,72–74] Therefore, the higher J_{sc} estimated in the present study is consistent with the results of short-circuit currents in the previous reports. To understand the recombination mechanisms in the proposed heterojunction multilayer structures, further study on the effect of radiative recombination on the photocurrent is necessary.

Figure 2b shows the energy band diagram of the proposed Sb₂Se₃-based solar cell with the SnS HTL. It is observed (in Figure 1b) that the addition of SnS HTL at the back side of the absorber in the conventional Sb₂Se₃-based solar cell exhibits low valence band offset between the absorber and the HTL, and this results in the smooth transport of holes from the absorber to back metal electrode. In addition, the higher conduction band offset at the Sb₂Se₃/SnS interface would create sufficient potential barrier to prevent the flow of the minority carriers (electrons) toward the back surface.

Moreover, a strong electric field at the back of the solar cell can be induced due to the formation of p⁺-p high-low junction by the introduction of p⁺-type SnS HTL at the back of the p-Sb₂Se₃ absorber,^[43,46] as shown in Figure 2c. This enhanced built-in electric potential along the absorber layer would not only be effective to reflect the minority electrons from the back surface, but also to boost the collection of the photogenerated electrons and holes. This would result in a significant increase in V_{oc} and J_{sc} and, hence, improve the overall performance by minimizing the carrier recombination at the back surface of the proposed solar cell.^[43,45,47]

The EQEs as a function of the wavelength of both FTO/CdS/Sb₂Se₃ and FTO/CdS/Sb₂Se₃/SnS heterojunction structures are also manifested in Figure 2d. It can be seen that higher quantum efficiency of the solar cell with HTL is obtained as compared with the cell without HTL. It is noted that the sharp decrease in EQE at the wavelength corresponding to the energy bandgap ($E_g = 1.06$ eV) is not observed. High spectral response at longer wavelength may also be attributed to notable absorption by the absorber as well as by the SnS HTL. The unabsorbed high energetic photons in the thin Sb₂Se₃ absorber layer might be absorbed by the SnS HTL, which gives an additional benefit in the cell performance. This result is consistent with the EQE results reported in the previous studies.^[50,73] Moreover, it is observed that the EQE at the wavelength ranged from 350 to 500 nm is high. This may be due to capture of more photons by the absorber layer in the short wavelength range. Thus, this absorbed incident photons would create a sufficient number of electron-hole pairs. The behavior of the EQE at the short wavelength range is similar to the simulation results reported in the previous works.^[50,73]

3.2. Influences of Thickness and Doping Concentration of ETL on Cell Performances

The CdS as an ETL is used in the proposed Sb₂Se₃-based TFSC. The performance parameters of the proposed solar cell are

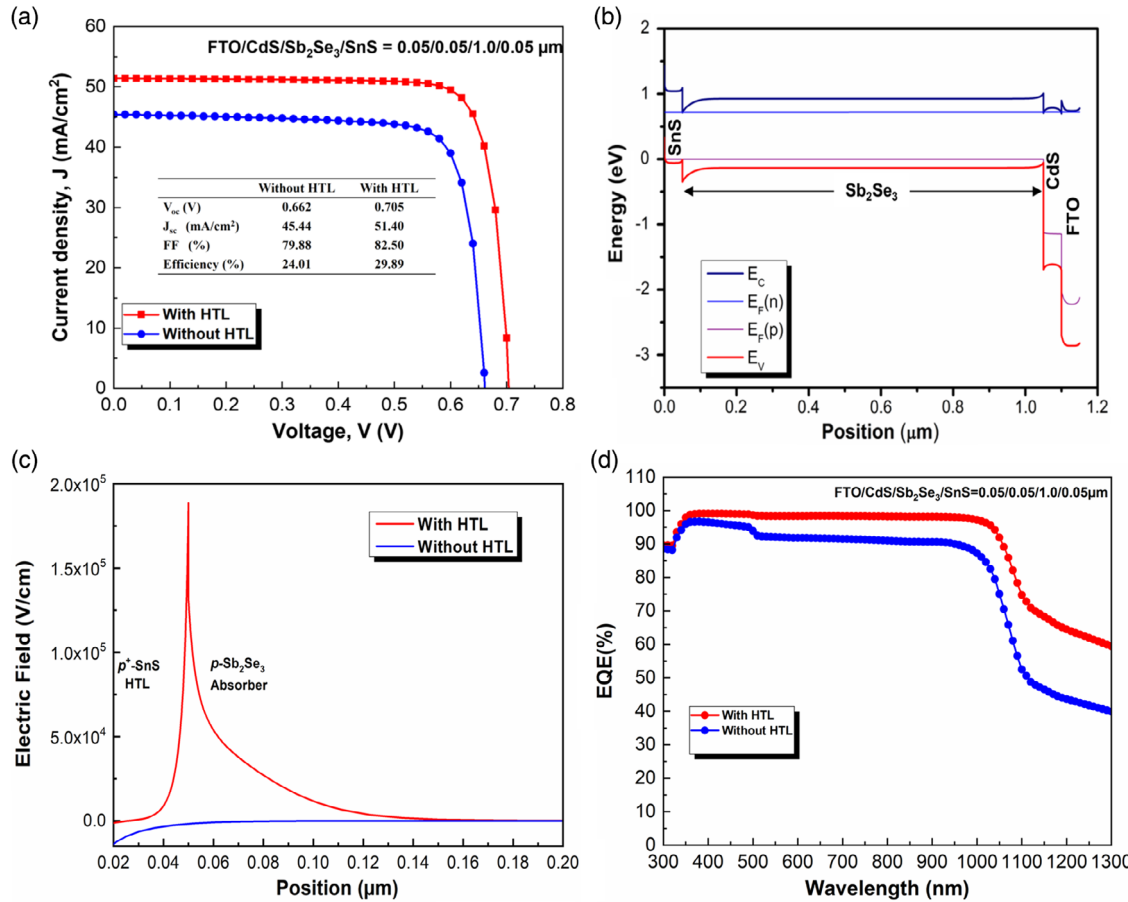


Figure 2. Simulated a) J - V characteristics, b) energy band diagram, c) electric field distribution at the absorber/HTL interface, and d) spectral response of the Sb_2Se_3 -based TFSCs.

analyzed as a function of the thickness of CdS ETL, as manifested in **Figure 3a**. The thickness of CdS is ranged from 0.01 to 0.1 μm , whereas the thicknesses of the TCO, absorber, and HTL are set at 0.05, 1.0, and 0.05 μm , respectively. It is seen in the simulation results that V_{oc} , J_{sc} , FF, and efficiency are almost uniform with increasing the ETL thickness. The influence of the various ETL thicknesses on the spectrum response, i.e., EQE of the proposed solar cell, is also presented in Figure 3b. It can be noted that there is no noticeable variation in the EQE values as a function of the ETL thickness. The minimal current due to the insufficient photoinduced charge carriers with thicker ETL may be responsible for the stable solar cell output characteristics.^[75] Therefore, a thin CdS ETL of 0.05 μm is optimized to get better photovoltaic performances in the following calculations. At the optimum ETL thickness of 0.05 μm , an efficiency of 29.89% with a V_{oc} of 0.705 V, a J_{sc} of 51.40 mA cm^{-2} , and an FF of 82.50% is estimated.

The effect of donor density of ETL layer has been investigated. Here, 1.0 μm -thick absorber layer (acceptor density: $1 \times 10^{17} \text{ cm}^{-3}$ and defect: $6.9 \times 10^{14} \text{ cm}^{-3}$) with 0.05 μm of HTL (acceptor density: $1 \times 10^{19} \text{ cm}^{-3}$ and defect: $1 \times 10^{15} \text{ cm}^{-3}$), 0.05 μm of ETL, and 0.05 μm of TCO is used to analyze the cell performances by varying the doping concentration of ETL. The donor density of ETL with a defect of $1 \times 10^{15} \text{ cm}^{-3}$ has been varied from

1×10^{12} to $1 \times 10^{20} \text{ cm}^{-3}$ at 300 K temperature for numerical calculations. **Figure 4** shows the output parameters of the proposed solar cell as a function of ETL doping concentration. It can be observed that all the output characteristics are remained almost constant with the increase in ETL donor density. Almost the same conversion efficiency of about 29.85% is obtained for the doping density in the range from 1×10^{12} to $1 \times 10^{20} \text{ cm}^{-3}$ donor concentration. In this numerical study, the ETL donor density of $1 \times 10^{17} \text{ cm}^{-3}$ has been taken for next investigations considering low cost of the solar cell manufacturing.

3.3. Effect of HTL on Cell Performances

3.3.1. Effect of Doping Concentration of HTL

The effect of the doping concentration of the SnS HTL on the photovoltaic performance of the proposed Sb_2Se_3 -based TFSC is studied. The numerical simulation outputs with variations of the HTL acceptor density are demonstrated in **Figure 5**. The acceptor density of HTL is shifted from 1×10^{12} to $1 \times 10^{20} \text{ cm}^{-3}$ with the fixed acceptor and donor densities of 1×10^{17} and $1 \times 10^{18} \text{ cm}^{-3}$ for the absorber and TCO layers, respectively. From the simulation results in **Figure 5a**, it can

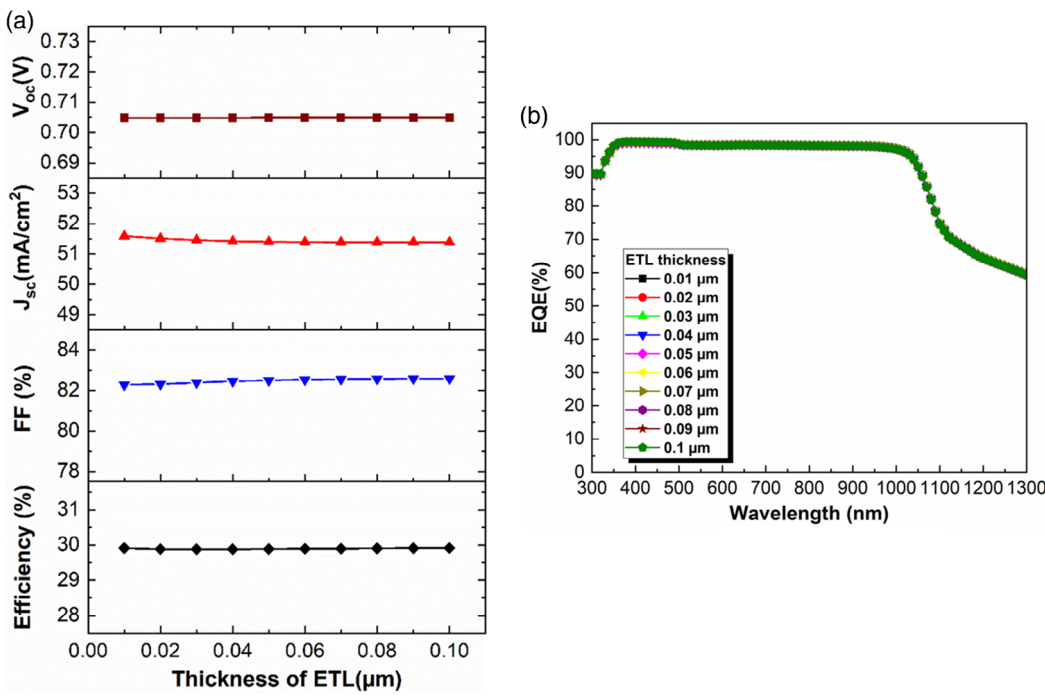


Figure 3. Influence of ETL thickness on a) performance parameters such as V_{oc} , J_{sc} , FF, and efficiency and b) EQE of the proposed Sb_2Se_3 -based TFSC.

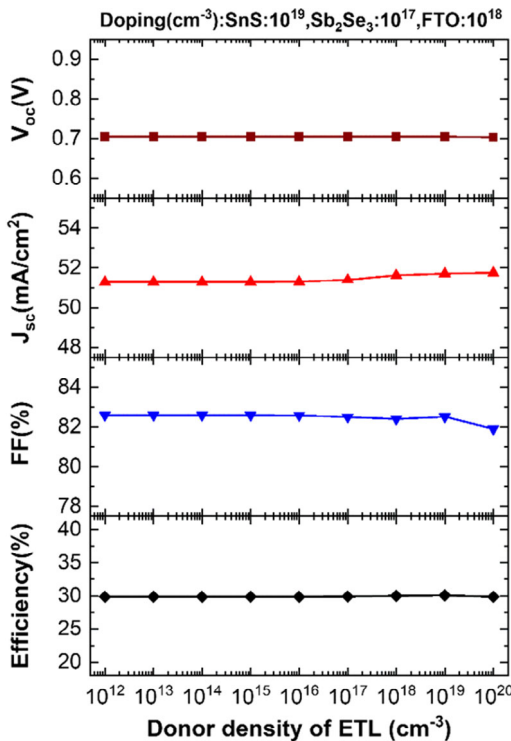


Figure 4. Simulated performances of V_{oc} , J_{sc} , FF, and efficiency of the proposed cell as a function of the donor density of ETL.

be observed that all the solar cell performance parameters such as V_{oc} , J_{sc} , FF, and efficiency are slightly improved with an increment of the HTL acceptor density. The conversion efficiency

from 29.72% to 30.04% is determined when the SnS doping density is boosted from 1×10^{12} to 1×10^{20} cm⁻³. In this numerical study, the HTL doping concentration is chosen to be 1×10^{19} cm⁻³.

This performance enhancement can be explained using the energy band diagram. Figure 5b describes the energy band diagram of the proposed Sb_2Se_3 -based TFSC depending on the doping concentration of the SnS HTL. The conduction and valence bands shift upward with raising the doping concentration of the SnS HTL, as shown in Figure 5b. As a result, a large built-in electric potential is developed between the HTL and the absorber interface at the high acceptor density.^[43,52,76]

The presence of the strong electric field at the absorber/HTL interface with the high doping concentration would contribute to increase the hole transportation from Sb_2Se_3 absorber to SnS HTL, and the flow of minority electrons can be minimized and, thus, reduces the carrier recombination rate.^[43] The carrier recombination rate of the Sb_2Se_3 -based TFSC with SnS HTL for the variations of the acceptor density of the HTL is plotted in Figure 5c. It can be further seen that the recombination rate in the absorber is declined for the high doping densities.^[77]

From the above-mentioned simulation results, it is revealed that the enhancement of the carrier transport properties and the drop of the carrier recombination rate in the Sb_2Se_3 absorber layer might result in the improvement of the solar cell performances.

3.3.2. Effect of HTL Thickness

To understand the performance, it is important to optimize the HTL thickness. In the present simulation study, the effect of the

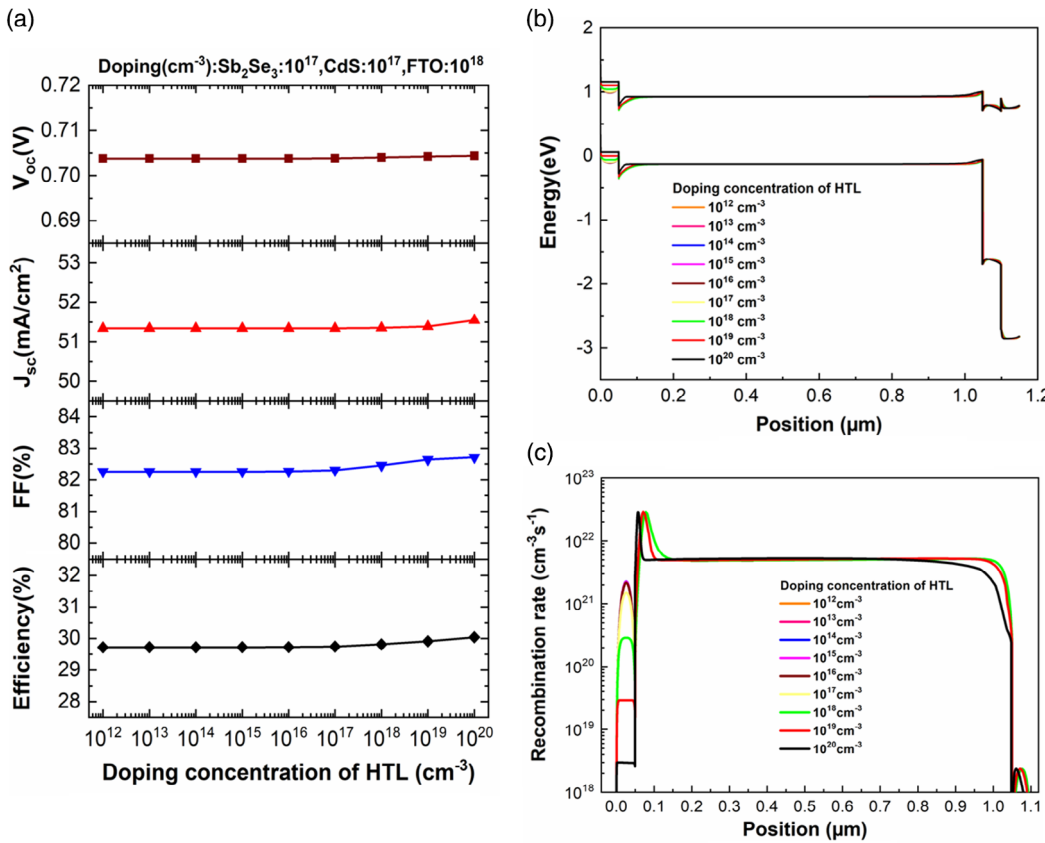


Figure 5. Effect of the acceptor density of the SnS HTL on the a) photovoltaic performance parameters, b) energy band structure, and c) carrier recombination rate profile of Sb_2Se_3 .

HTL thickness varied from 0.01 to 0.1 μm on performance parameters such as V_{oc} , J_{sc} , FF, and efficiency of the proposed Sb_2Se_3 solar cell is investigated, as shown in Figure 6. It can be found that the all the solar cell output parameters show negligible changes up to a thickness of 0.05 μm , and a slight increase in the conversion efficiency is noticed when the HTL thickness exceeds 0.05 μm . The optimized HTL thickness for improving the light harvesting is selected to be 0.05 μm by considering the cost of cell production.

3.3.3. Effect of Electron Affinity of HTL

To understand the contact condition of semiconducting heterojunction, in the present work, the impact of HTL electron affinity on the performances and characteristics of the solar cells is also analyzed, as displayed in Figure 7. The electron affinity of HTL is varied from 3.3 to 3.7 eV, whereas the other material parameters are remained stable. Figure 7a shows the J - V curves of the Sb_2Se_3 solar cell for the various electron affinity of HTL. It is revealed that the values of V_{oc} and J_{sc} increase significantly when the HTL electron affinity varies from 3.3 to 3.5 eV and then are almost saturated with rising the electron affinity above 3.5 eV. The corresponding conversion efficiencies of 23.73% and 30.67% are estimated for the affinities of 3.3 and 3.7 eV, respectively. Thus, with the electron affinity of HTL larger than 3.5 eV,

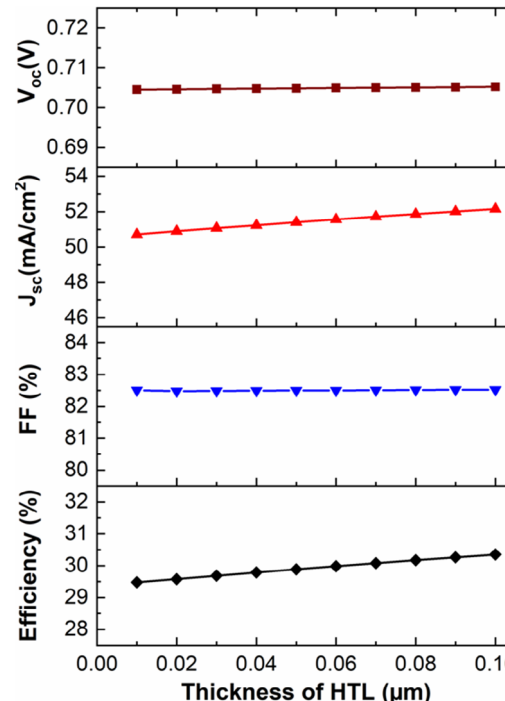


Figure 6. Effect of the HTL thickness on performance parameters such as V_{oc} , J_{sc} , FF, and efficiency of the proposed Sb_2Se_3 solar cell.

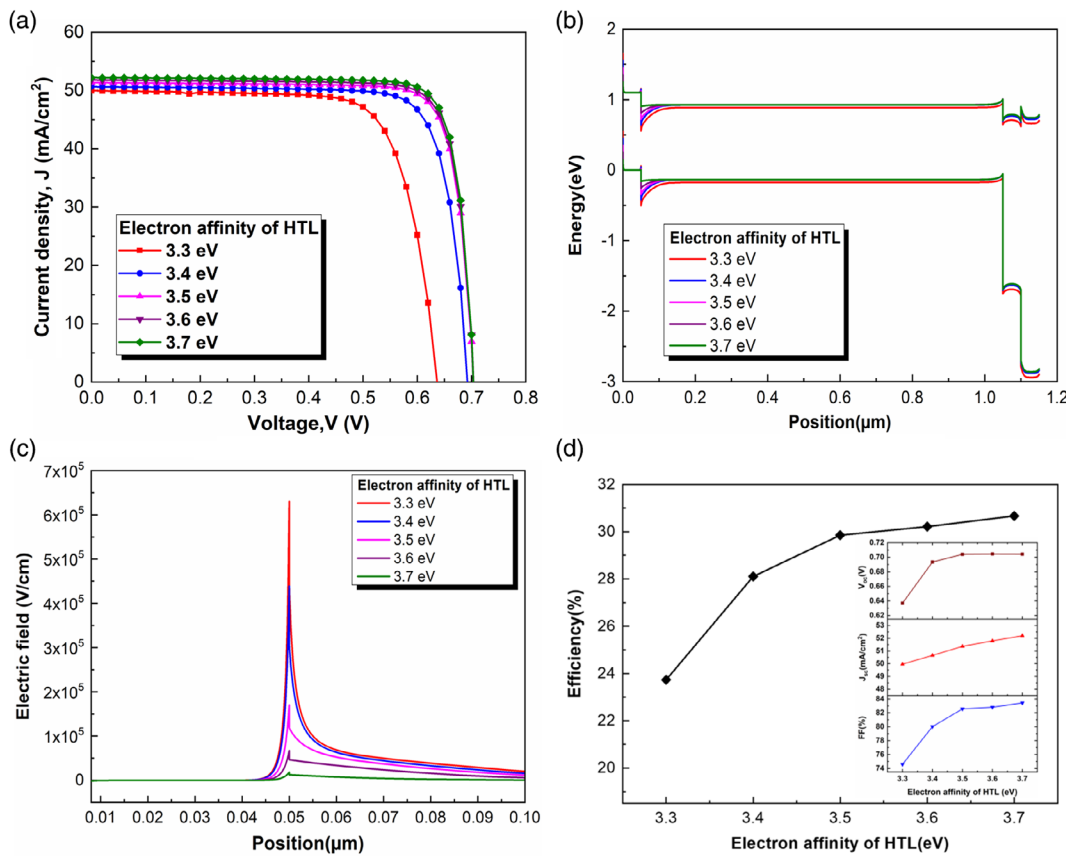


Figure 7. Impact of HTL electron affinity on the a) J – V characteristics, b) energy band diagrams, c) electric field distribution, and d) performance parameters of the Sb_2Se_3 solar cell.

the overall photovoltaic performances of the Sb_2Se_3 solar cell can be enhanced. Figure 7b shows the energy band diagram of Sb_2Se_3 solar cell with different electron affinity of HTL. As shown in Figure 7b, the transport of holes across the heterojunction can be enhanced with increasing the HTL electron affinity. The potential energy barrier between the HTL and the absorber is heightened by the reduction of the HTL electron affinity. At low affinity, large potential barrier is formed against the holes at the absorber/HTL interface and, hence, enhances the probability of the electron–hole recombination.^[43] The electric field distribution at the absorber/HTL interface is also presented in Figure 7c. Therefore, the minimization of the recombination loss at the absorber/HTL interface with the HTL electron affinity larger than 3.5 eV may lead to improve the photovoltaic performance parameters, as manifested in Figure 7d. Hence, in the present study, the suitable electron affinity value of 3.52 eV for the SnS as an HTL is used to attain the optimal conversion efficiency of the Sb_2Se_3 solar cell.

3.4. Effect of Thickness of Absorber on Cell Performances

The absorber thickness plays a crucial role to understand the performance of the thin-film heterojunction solar cells. In this numerical study, a comparison of the performance parameters of the Sb_2Se_3 -based solar cell without and with HTL is also

explored by varying the absorber thickness at an operating temperature of 300 K. Figure 8a exhibits the photovoltaic parameters such as V_{oc} , J_{sc} , FF, and efficiency as a function of the absorber layer thickness of the Sb_2Se_3 -based solar cell without and with HTL. The thickness of the Sb_2Se_3 absorber in both the solar cells is ranged from 0.1 to 2.0 μm . As evident from Figure 8a, it can be noticed that all the output parameters of the cell with the SnS HTL are superior to the solar cell without HTL. It is also seen that the simulated photovoltaic parameters in both cells are increased slowly beyond the absorber thickness of 1.0 μm . The deviation of V_{oc} is detected in both solar structures. At 1.0 μm -thick absorber layer, a higher V_{oc} of 0.705 V for the cell with the SnS HTL is calculated than a V_{oc} of 0.662 V for the device without HTL. A J_{sc} of 51.40 mA/cm^2 is determined for the solar cell with HTL at the Sb_2Se_3 absorber thickness of 1.0 μm , which is larger than a J_{sc} of 45.44 mA/cm^2 found for the cell without HTL. The rise in V_{oc} and J_{sc} would boost the efficiency of the solar cell. Higher FF in the proposed solar cell is revealed than the FF measured in the reference structure without HTL. The values of FF for the Sb_2Se_3 -based solar cell with and without HTL are computed to be 82.50% and 79.88%, respectively, at the same 1.0 μm -thick Sb_2Se_3 layer. As also shown in Figure 8a, the efficiencies in both the Sb_2Se_3 -based solar cells are improved with increasing the Sb_2Se_3 absorber thickness. The efficiencies of 20.49% and

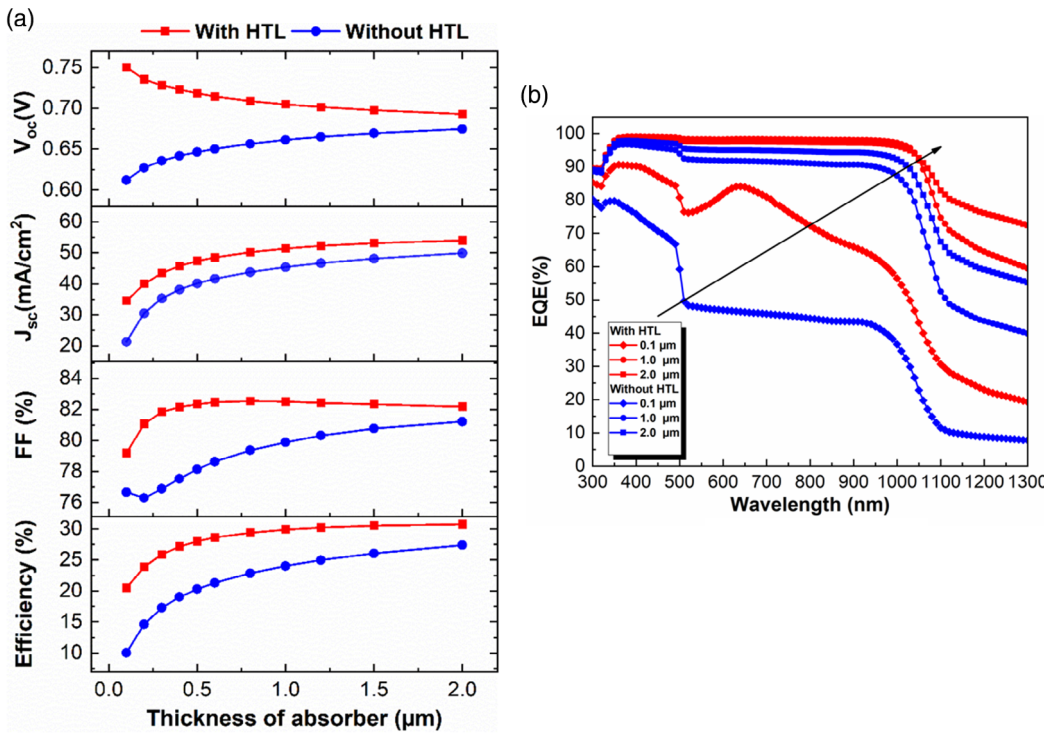


Figure 8. Effect of thickness of the absorber layer on the a) performance parameters and b) spectral response of the Sb_2Se_3 -based solar cell without and with HTL.

29.89% in the proposed device have been calculated at the Sb_2Se_3 thicknesses of 0.1 and 1.0 μm, respectively; on the other hand, the efficiencies of the cell without HTL are evaluated to be 10.03% and 24.01%, respectively. It is suggested that the reflection of minority electrons from the back surface to front contact due to the strong built-in potential at the absorber/HTL interface as well as the reduced barrier for the transport of holes from absorber to HTL result in the higher efficiency of the Sb_2Se_3 -based TFSC with SnS HTL. In the present work, the Sb_2Se_3 absorber thickness of 1.0 μm is selected as the optimize value considering the device cost.

Figure 8b plots the spectral response as a function of wavelength for the Sb_2Se_3 -based solar cells of Al/FTO/ETL/ Sb_2Se_3 /Mo and Al/FTO/ETL/ Sb_2Se_3 /HTL/Mo. The quantum efficiencies of both the solar structures are shown at the absorber thicknesses of 0.1, 1.0, and 2.0 μm, respectively. It is evident that higher quantum efficiency with the increment of absorber thickness is recorded, and this is may be due to the increase of photon absorption with the rise of absorber thickness. It is also revealed in Figure 8b that better EQE can be achieved in the Sb_2Se_3 -based solar cell using the SnS HTL as compared with that of the cell without HTL. The reduced carrier recombination rate at the HTL/absorber interface results in the performance enhancement of the proposed solar cell. The explanations about the carrier recombination currents in both the solar cells are provided in the following paragraph.

The carrier recombination current densities inside the both solar cells are calculated from the current–voltage characteristics. Figure 9 shows the calculated carrier recombination current densities in both the solar cells with the variations of cell voltage. It can be found that the minority carrier recombination current at

back side and the total carrier recombination current in the proposed solar cell are comparatively lower than the reference cell.^[50,78] Therefore, these results lead to suggest that the insertion of the SnS HTL between the absorber and the back metal contact would be effective to reduce the carrier recombination loss inside the Sb_2Se_3 -based solar cell.

3.5. Effect of Doping Concentration of Absorber on Cell Performances

Figure 10 shows the output parameters of the proposed device as a function of acceptor density of the Sb_2Se_3 absorber. In this simulation, the acceptor density of the absorber layer is expanded from 1×10^{12} to $1 \times 10^{20} \text{ cm}^{-3}$, whereas the fixed doping density mentioned in Table 1 for CdS, FTO, and SnS, respectively, has been used. As can be observed in Figure 10, all the photovoltaic parameters such as V_{oc} , J_{sc} , FF, and efficiency are almost constant up to the doping density of $1 \times 10^{15} \text{ cm}^{-3}$. V_{oc} remains constant till $1 \times 10^{15} \text{ cm}^{-3}$ and then increases linearly with the acceptor density. The values of 0.62 and 0.86 V are obtained at 1×10^{12} and $1 \times 10^{20} \text{ cm}^{-3}$, respectively. J_{sc} is calculated to be 53.24 mA cm^{-2} at $1 \times 10^{12} \text{ cm}^{-3}$ and then is degraded to 48.56 mA cm^{-2} at $1 \times 10^{20} \text{ cm}^{-3}$. The values of FF are expanded from 61.63% to 86.70% for the density in the range from 1×10^{12} to $1 \times 10^{20} \text{ cm}^{-3}$. It can be further seen that the conversion efficiency of the proposed solar cell is enhanced linearly beyond the absorber acceptor density of $1 \times 10^{15} \text{ cm}^{-3}$. The combining enhancement effects of V_{oc} and FF result in the improvement in efficiency with the acceptor density. These results are in good agreement with the performances reported in the previous

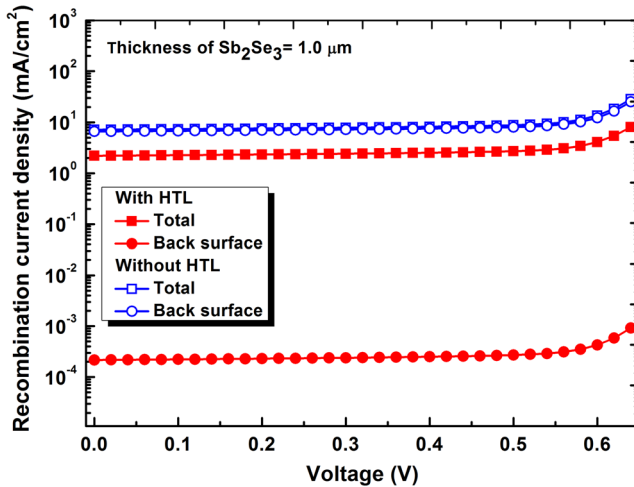


Figure 9. Calculated carrier recombination current densities in both the solar cells with the variations of cell voltage.

study.^[79] The conversion efficiencies of the Sb₂Se₃-based solar cell with SnS HTL are evaluated to be 20.30% and 36.74% at the densities of 1 × 10¹² and 1 × 10²⁰ cm⁻³, respectively.

3.6. Effect of Bulk Defect Density of Absorber on Cell Performances

The photovoltaic energy conversion is greatly influenced by the condition of the absorber layer. High defect states in the film may

enhance the probability of the carrier recombination rate and, thus, deteriorate the overall solar cell performances. In the present work, the influence of the Sb₂Se₃ defect density on the cell performances is analyzed. **Figure 11** presents the variation of performance parameters of the proposed cell as a function of bulk defect density of the Sb₂Se₃ layer. In this numerical calculation, the bulk defect density of absorber is shifted from 1 × 10¹² to 1 × 10¹⁷ cm⁻³ with the TCO, ETL, absorber, and HTL thicknesses of 0.05, 0.05, 1.0, and 0.05 μm, respectively. The defect densities of other materials are fixed and mentioned in Table 1. As shown in Figure 11, all the photovoltaic parameters are in decreasing approach with the increase in the absorber defect density. This result may be due to the boost of recombination of the photogenerated carriers before reaching the external circuit at the high defect density.^[52,80] V_{oc} is decreased drastically from 0.86 to 0.50 V with the enhancement of bulk defect density in the absorber. The values of J_{sc} from 53.55 to 39.91 mA cm⁻² are observed for the bulk defect density in the range from 1 × 10¹² to 1 × 10¹⁷ cm⁻³. The FF reduces from 85.91% to 47.90%, whereas the efficiency declines from 39.55% to 9.60% for the defined range of defect density in Figure 11. According to the simulation results, it can be noticed that J_{sc} , FF, and efficiency of the proposed solar cell with SnS HTL are changed slightly for the defect density below 1 × 10¹⁵ cm⁻³. Thus, it is expected to take a low defect density of the absorber layer.

To optimize the performance of the Sb₂Se₃-based solar cell with SnS HTL, in this work, the bulk defect density in the Sb₂Se₃ layer has been considered to be 6.9 × 10¹⁴ cm⁻³. This

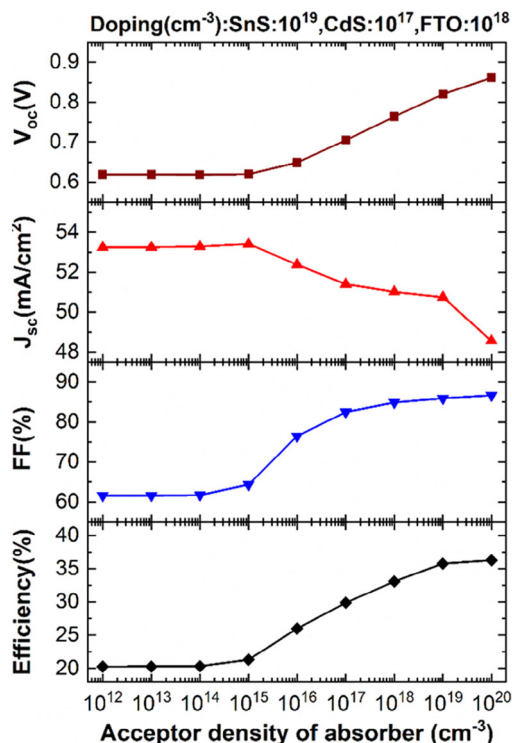


Figure 10. Output parameters of the proposed device as a function of acceptor density of the Sb₂Se₃ absorber.

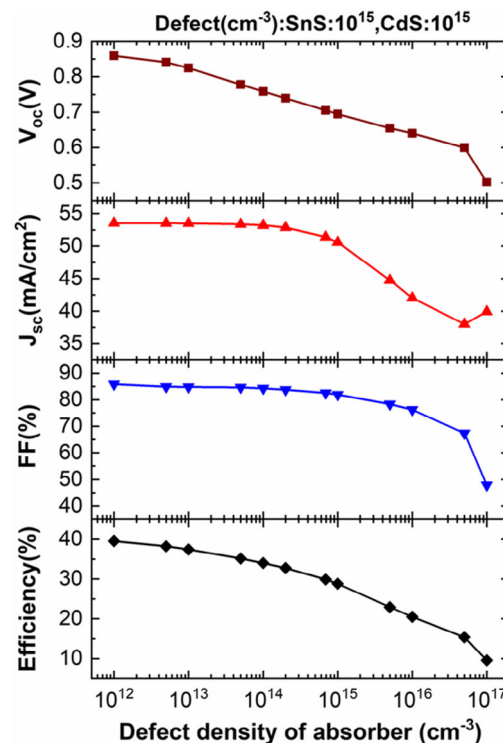


Figure 11. Variation of performance parameters of the proposed cell as a function of bulk defect density of the Sb₂Se₃ layer.

result is consistent with the total defect states measured for the Sb_2Se_3 absorber material in the previous report.^[25,50] The conversion efficiency of 29.89% at $6.9 \times 10^{14} \text{ cm}^{-3}$ for the proposed solar cell is determined.

3.7. Effect of Interface Defect on Cell Performances

3.7.1. Effect of ETL/Absorber Interface Defect Density

The performances of the solar cell are also strongly affected by the defects at interfaces in the heterojunction structures. In the numerical study, the influence of the defect density at the ETL/absorber interface is investigated on the performance parameters of the proposed Sb_2Se_3 -based solar cell. Figure 12a indicates the simulation results for the solar cell output parameters as a function of the defect density at the $\text{CdS}/\text{Sb}_2\text{Se}_3$ interface in the range from 1×10^8 to $1 \times 10^{18} \text{ cm}^{-2}$. It can be demonstrated that the device performance parameters such as V_{oc} , FF, and efficiency are declined with increasing the defect concentration at the ETL/absorber interface, whereas the value of J_{sc} of the proposed solar cell remains about unaffected. The series resistance may also be increased significantly with the increment of interface defect.^[81] However, the series resistance does not have great effect on J_{sc} , thus resulting in the almost constant J_{sc} with the variation of defect density at ETL/absorber interface. The conversion efficiencies of 29.92% and 13.01% are calculated at the defect densities of 1×10^8 and $1 \times 10^{18} \text{ cm}^{-2}$, respectively. This deteriorate in performances is due to the enhancement in the carrier recombination rate at the interface with increasing the defect density.^[52,82,83] Thus, it is suggested that the defects at the ETL/absorber interface have significant role on the performance parameters of the photovoltaic devices.^[43,50,80,84]

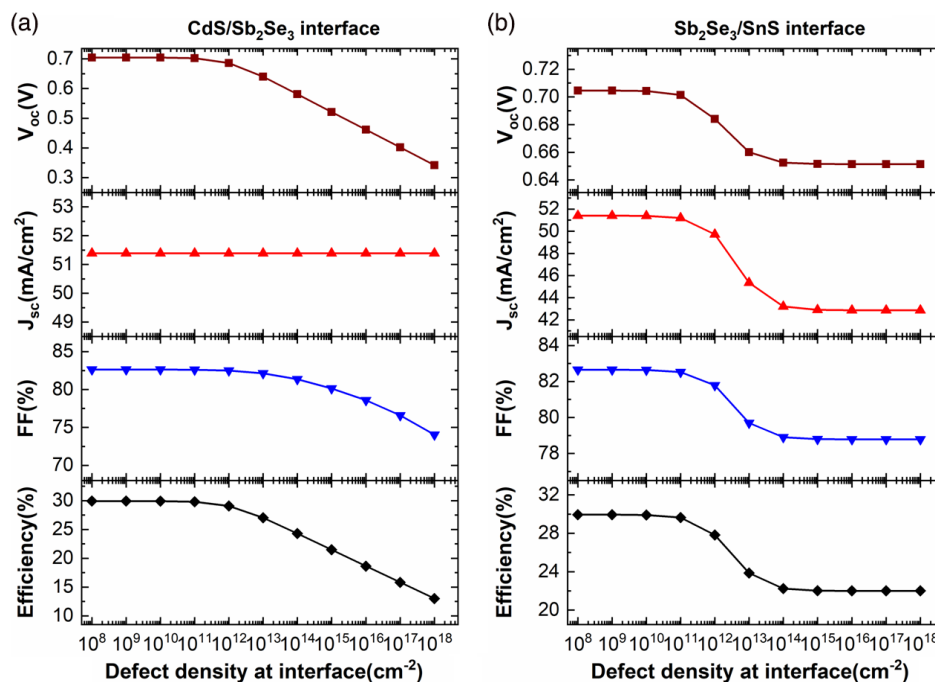


Figure 12. Effect of defect density at the a) $\text{CdS}/\text{Sb}_2\text{Se}_3$ and b) $\text{Sb}_2\text{Se}_3/\text{SnS}$ interfaces on the photovoltaic performance parameters.

3.7.2. Effect of Absorber/HTL Interface Defect Density

To observe the impact of the defects at the second interface between Sb_2Se_3 and SnS on the proposed solar cell output parameters, in the present numerical investigation, the simulation has been done by shifting the defect density from 1×10^8 to $1 \times 10^{18} \text{ cm}^{-2}$. The calculated photovoltaic performance parameters of the Sb_2Se_3 -based solar cell with SnS HTL are presented in Figure 12b. As can be evident from the simulation results, all the solar cell output parameters are almost stable up to the defect density of $1 \times 10^{11} \text{ cm}^{-2}$ and then gradually degrade under the defect of $1 \times 10^{15} \text{ cm}^{-2}$. As the defect density at absorber/HTL interface exceeds $1 \times 10^{14} \text{ cm}^{-2}$, the photovoltaic parameters remain constant with a further increase in the defect density, as shown in Figure 12b. The conversion efficiency drops from 29.94% to 22.00% for the interface defect density incremented from 1×10^8 to $1 \times 10^{18} \text{ cm}^{-2}$.

It is revealed that the performance parameters of the photovoltaic heterojunction structures are greatly affected by the defects at the ETL/absorber interface than at the absorber/HTL interface.^[50,52] In this simulation work, the values of the defect density at both the $\text{CdS}/\text{Sb}_2\text{Se}_3$ and $\text{Sb}_2\text{Se}_3/\text{SnS}$ interfaces are set at $1 \times 10^{10} \text{ cm}^{-2}$ to achieve the best power conversion efficiency.

3.8. Effect of Working Temperature and Back Metal Contact Work Function on Cell Performances

In this study, the solar cell characteristics are investigated by varying an operating temperature from 260 to 475 K. Figure 13a shows the performance parameters for both the cell with and without HTL as a function of the operating

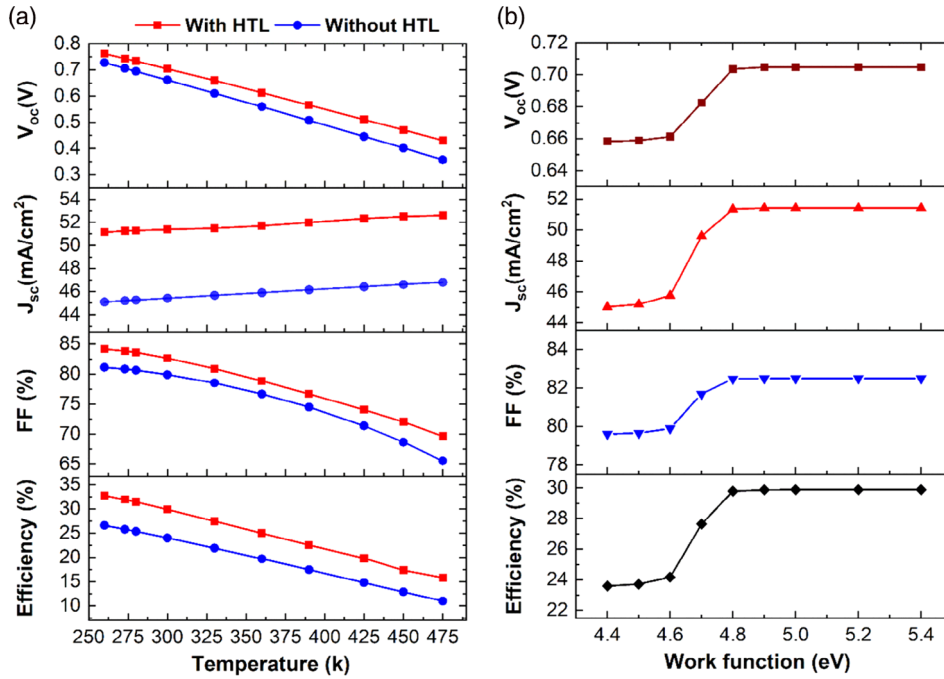


Figure 13. a) Output parameters such as V_{oc} , J_{sc} , FF, and efficiency of the Sb_2Se_3 -based solar cell without and with HTL as a function of the operating temperature. b) Effect of back contact metal work function on the output parameters of FTO/ETL/ Sb_2Se_3 /HTL solar cells.

temperature. As can be observed in Figure 13a, the performance parameters such as V_{oc} , FF, and efficiency are in diminution nature with increasing the temperature for both the solar structures, whereas the values of J_{sc} are increased slightly with the operating temperature. The decreasing of energy bandgap of materials by variation of the temperature might result in the slight increment of the short-circuit current in the semiconductors-based heterojunction TFSCs.^[50,85–87] Thus, the degradations of the FF and the efficiency are due to combined effects of the drop in V_{oc} and the rise in J_{sc} , as shown in Figure 13a. The conversion efficiencies of 32.77% and 15.79% are obtained for the Sb_2Se_3 -based solar cell with SnS HTL at 260 and 475 K, respectively. On the other hand, the lower efficiencies in case of the reference Sb_2Se_3 -based solar structure without HTL than the proposed cell are estimated to be 26.6% and 10.95%, respectively. Hence, it is revealed that the insertion of HTL into the reference Sb_2Se_3 heterojunction structure also enhances the stability of the photovoltaic device with changing the operating temperature.

The role of back metal contact work function on the output parameters of the proposed solar structure of Al/FTO/ETL/ Sb_2Se_3 /HTL/Mo is also studied, as demonstrated in Figure 13b. To get a suitable back contact for the proposed device, the simulation has been done with the back metal contact work function varied from 4.4 to 5.4 eV. In Figure 13b, it is found that all the photovoltaic parameters increase significantly with expand of the work function up to 4.9 eV. When the work function exceeds 4.9 eV, V_{oc} , J_{sc} , FF, and efficiency are saturated. It is clear that the output parameters of the proposed solar cell greatly depend on the back metal contact work function less than or equal to 4.9 eV. The potential barrier generated at the SnS/back contact interface decreases on increasing the back metal contact

work function. This leads to enhance the photovoltaic performances. Therefore, a suitable work function of greater than 4.9 eV for the back metal contact should be considered to get better photovoltaic performances. In the present numerical model, Mo as the back contact having work function of 4.95 eV has been used to realize the highly efficient Sb_2Se_3 -based heterojunction solar cell.

3.9. Effect of Series and Shunt Resistances on Cell Performances

The device performances are significantly affected by two crucial parameters series (R_s) and shunt (R_{sh}) resistances. R_s of the solar cell mainly results from the circuit terminal and right-hand and left-hand side metal contacts.^[88] On the other hand, R_{sh} appears to be due to the reverse saturation current. In this simulation study, the influences of R_s and R_{sh} are examined using the SCAPS-1D simulator to analyze the photovoltaic performance of the proposed Sb_2Se_3 -based solar cell. Figure 14a shows the photovoltaic performance parameters as a function of R_s . R_s is changed from 0 to $6 \Omega \text{ cm}^2$, keeping R_{sh} constant at $10^5 \Omega \text{ cm}^2$. It can be seen that V_{oc} is almost independent of R_s . In Figure 14a, J_{sc} , FF, and efficiency are degraded sharply with increasing R_s . The efficiencies of the Sb_2Se_3 solar cell with HTL are recorded to be 29.88% and 17.03% for 0 and $6 \Omega \text{ cm}^2$, respectively. This reduction in the photovoltaic performances may be due to the power loss at high R_s . Therefore, low series resistance is very much desirable.

The effect of R_{sh} on the cell performance is also explored. R_{sh} is varied from 30 to $1 \times 10^7 \Omega \text{ cm}^2$ with the fixed R_s of $0.5 \Omega \text{ cm}^2$. Figure 14b reveals solar cell output parameters as a function of R_{sh} . It can be noticed from the simulation results that all the

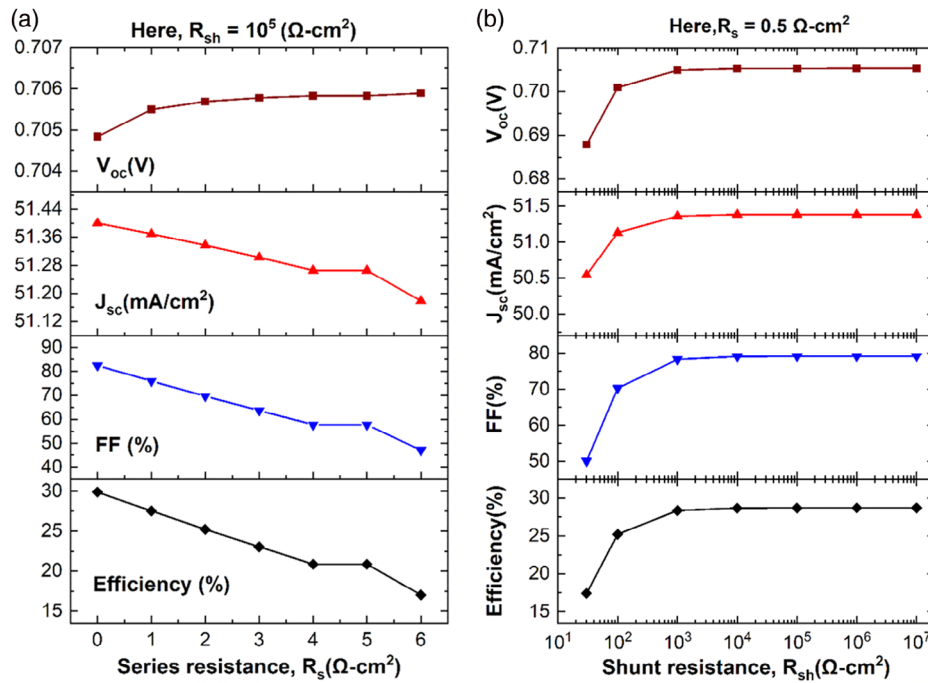


Figure 14. Variations of the performance parameters such as V_{oc} , J_{sc} , FF, and efficiency of the Sb_2Se_3 -based solar cell with HTL as a function of a) series (R_s) and b) shunt (R_{sh}) resistances.

photovoltaic parameters start growing significantly with the increase in R_{sh} till $10^3 \Omega \cdot \text{cm}^2$. It is also found that the photovoltaic performance parameters are almost unaffected by R_{sh} larger than $10^3 \Omega \cdot \text{cm}^2$. The achieved results are shown the same trend reported in the previous studies.^[50,89,90] It is, thus, revealed that low series resistance has significant influence on the cell performances.

3.10. Photovoltaic Performance of Sb_2Se_3 Solar Cells

Table 3 represents the performance parameters of the Sb_2Se_3 TFSCs with HTL evaluated in the previous and present works.^[34,37,43–45,47] The present work studies the performances of the Al/FTO/CdS/ Sb_2Se_3 /Mo and Al/FTO/CdS(ETL)/ Sb_2Se_3 /SnS(HTL)/Mo heterojunction structures. It is revealed from the simulation results that the overall performance of

the conventional Sb_2Se_3 solar cell without HTL is notably influenced by the carrier recombination at the back side. The conversion efficiency of the Al/FTO/CdS/ Sb_2Se_3 /Mo heterojunction solar device is obtained to be 24.01% in case of 1.0 μm absorber layer. On the contrary, the boosted efficiency of 29.89% at 1.0 μm -thick absorber layer is obtained for the proposed solar cell with HTL. Thus, the incorporation of an ultrathin SnS HTL of 0.05 μm into the basic Sb_2Se_3 -based heterojunction solar cell would be effective to minimize the minority carrier recombination loss at the back surface and, hence, enhance the overall performances of the solar cells. Moreover, the optimum energy bandgap, high absorption coefficient, high carrier mobility, non-toxic, and earth-abundant natures make the SnS material as a promising candidate to use as the HTL in the thin-film heterojunction solar cells. This numerical modeling and analysis would help the design engineers and researchers to manufacture and

Table 3. Performance parameters of the Sb_2Se_3 TFSCs with HTL evaluated in the previous and present works.

Structures	Field of research	V_{oc} [V]	J_{sc} [mA cm^{-2}]	FF [%]	Efficiency [%]	Ref.
ITO/CdS/ Sb_2Se_3 /PbS(HTL)/Au	Exp.	0.427	25.5	59.3	6.5	[34]
ITO/CdS/ Sb_2Se_3 /CuSCN(HTL)/Au	"	0.413	30.51	58.99	7.5	[37]
Ag/phenyl-C61-butyric acid methyl ester (PCBM)/ Sb_2Se_3 /HTL/ITO	Theo.	0.858	34.18	84.04	24.66	[43]
ITO/ In_2S_3 / Sb_2Se_3 / Cu_2O (HTL)/carbon nanotube (CNT)	"	0.67	26.84	79.74	13.20	[44]
FTO/CdS/ Sb_2Se_3 /CuO(HTL)/Au	"	0.643	33.54	74.43	16.06	[45]
FTO/Zn(Sn,O)/ Sb_2Se_3 /CZTSe(HTL)/Au	"	0.66	34.66	81.18	18.50	[47]
Al/FTO/CdS(ETL)/ Sb_2Se_3 /SnS(HTL)/Mo	"	0.705	51.40	82.50	29.89	a)

a) Indicates proposed cell.

fabricate highly efficient thin-film heterojunction solar cells based on semiconductor materials.

4. Conclusion

In this work, the performances of the thin-film heterojunction solar cells based on Sb_2Se_3 semiconductor absorber have been investigated using the SCAPS-1D simulation software. To enhance the overall performance of conventional Sb_2Se_3 solar cell, the inorganic SnS semiconductor material as an HTL is proposed and integrated at the back contact of the cell. The numerical modeling has been carried out to evaluate and analyze the impacts of the thickness and doping concentration of absorber, ETL, and HTL, electron affinity of HTL, bulk defect of absorber, and working temperature, back metal contact work function, and series and shunt resistances on the cell performances. Optimum results have been found with the minimal thickness of 0.05, 0.05, and $1.0 \mu\text{m}$ for FTO, CdS, and Sb_2Se_3 , respectively. The doping density of $1 \times 10^{17} \text{ cm}^{-3}$ is chosen for both CdS ETL and Sb_2Se_3 absorber. The conversion efficiency of the Sb_2Se_3 -based TFSC without HTL is obtained to be 24.01%. According to the simulation results, it is found that the carrier recombination at the back side of the conventional Sb_2Se_3 solar cell influences the photovoltaic performances greatly. In addition, it is revealed that the proposed device structure that consists of Al/FTO/CdS(ETL)/ Sb_2Se_3 /SnS(HTL)/Mo improves the solar cell output parameters by minimizing the recombination loss at the back surface. In the case of the absorber bulk defect density and the acceptor concentration at 6.9×10^{14} and $1 \times 10^{17} \text{ cm}^{-3}$, the enhanced efficiency of 29.89% ($J_{sc} = 51.40 \text{ mA cm}^{-2}$, $V_{oc} = 0.705 \text{ V}$, and FF = 82.50%) of the Sb_2Se_3 -based solar cell with a $0.05 \mu\text{m}$ ultra-thin SnS HTL is estimated. It is important to note that the values of the back contact metal work function (above 4.9 eV) and the electron affinity of HTL (larger than 3.5 eV) selected in this simulation work are appropriate to form sufficient potential barrier to achieve the better performance parameters of the Sb_2Se_3 solar cell. Moreover, the effect of defect density at the CdS/ Sb_2Se_3 and Sb_2Se_3 /SnS interfaces on the photovoltaic performance parameters has been studied. The best power conversion efficiency of 29.9% has been achieved with the defect density of $1 \times 10^{10} \text{ cm}^{-2}$ set at both the ETL/ Sb_2Se_3 and Sb_2Se_3 /HTL interfaces. It is further observed that better thermal stability can be achieved with the proposed device structure. Therefore, it is expected that this design configuration can be the appropriate guiding rules to develop highly efficient, low-toxic, and low-cost thin-film heterojunction solar cells.

Acknowledgements

The authors would like to thank Prof. Dr. Marc Burgelman and his colleagues at the Department of Electronics and Information Systems (ELIS), University of Gent, Belgium, for providing the SCAPS-1D software.

Conflict of Interest

The authors declare no conflict of interest.

Data Availability Statement

Research data are not shared.

Keywords

device efficiency, hole transport layers, Sb_2Se_3 solar cells, SCAPS-1D (solar cell capacitance simulator in 1D), tin sulfide

Received: January 21, 2021

Revised: March 29, 2021

Published online:

- [1] K. L. Chopra, P. D. Paulson, V. Dutta, *Prog. Photovolt. Res. Appl.* **2004**, 12, 69.
- [2] N. Amin, K. Sopian, M. Konagai, *Sol. Energy Mater. Sol. Cells* **2007**, 91, 1202.
- [3] N. R. Paudel, K. A. Wieland, A. D. Compaan, *Sol. Energy Mater. Sol. Cells* **2012**, 105, 109.
- [4] W. Liu, J. J. He, Z. G. Li, W. L. Jiang, J. B. Pang, Y. Zhang, Y. Sun, *Phys. Scr.* **2012**, 85, 055806.
- [5] L. A. Kosyachenko, X. Mathew, P. D. Paulson, V. Y. Lytvynenko, O. L. Maslyanchuk, *Sol. Energy Mater. Sol. Cells* **2014**, 130, 291.
- [6] I. Abdo, C. Trompoukis, L. Tous, V. Depauw, R. Guindri, I. Gordon, O. E. Daif, *IEEE J. Photovolt.* **2015**, 5, 1319.
- [7] M. D. Chatzisideris, N. Espinosa, A. Laurent, F. C. Krebs, *Sol. Energy Mater. Sol. Cells* **2016**, 156, 2.
- [8] P. Jackson, R. Wuerz, D. Hariskos, E. Lotter, W. Witte, M. Powalla, *Phys. Status Solidi RRL* **2016**, 10, 583.
- [9] T. D. Lee, A. U. Ebong, *Renew. Sustain. Energy Rev.* **2017**, 70, 1286.
- [10] Y. Cao, Y. Liu, J. Zhou, Y. Wang, J. Ni, J. Zhang, *Sol. Energy Mater. Sol. Cells* **2016**, 151, 1.
- [11] M. Xu, T. Bearda, H. S. Radhakrishnan, S. K. Jonnak, M. Hasan, S. Malik, M. Filipic, V. Depauw, K. Van Nieuwenhuyse, Y. Abdulraheem, M. Debucquoy, I. Gordon, J. Szlufcik, J. Poortmans, *Sol. Energy Mater. Sol. Cells* **2017**, 165, 82.
- [12] M. Powalla, S. Paetel, E. Ahlsweide, R. Wuerz, C. D. Wessendorf, T. M. Friedlmeier, *Appl. Phys. Rev.* **2018**, 5, 041602.
- [13] L. Et-taya, T. Ouslimane, A. Benami, *Solar Energy* **2020**, 201, 827.
- [14] Y. Cao, X. Zhu, X. Tong, J. Zhou, J. Ni, J. Zhang, J. Pang, *Front. Chem. Sci. Eng.* **2020**, 14, 997.
- [15] Y. O. Mayon, T. P. White, R. Wang, Z. Yang, K. R. Catchpole, *Phys. Status Solidi A* **2016**, 213, 108.
- [16] E. B. Salgado, L. A. R. Guadarrama, M. L. R. Garcia, L. G. Martinez, M. T. S. Nair, P. K. Nair, *Phys. Status Solidi A* **2017**, 214, 1700036.
- [17] L. Luo, W. Luan, B. Yuan, C. Zhang, L. Jin, *Energy Proc.* **2018**, 75, 2181.
- [18] D. J. Xue, B. Yang, Z. K. Yuan, G. Wang, X. Liu, Y. Zhou, L. Hu, D. Pan, S. Chen, J. Tang, *Adv. Energy Mater.* **2018**, 5, 1501203.
- [19] T. M. Razakov, G. S. Boltaev, A. Bosio, B. Ergashev, K. M. Kouchkarov, N. K. Mamarasulov, A. A. Mavlonov, A. Romeo, N. Romeo, O. M. Tursunkulov, R. Yuldasheva, *Sol. Energy* **2018**, 159, 834.
- [20] Y. Zhou, M. Leng, Z. Xia, J. Zhong, H. Song, X. Liu, B. Yang, J. Zhang, J. Chen, K. Zhou, J. Han, Y. Cheng, J. Tang, *Adv. Energy Mater.* **2014**, 4, 1301846.
- [21] Y. C. Choi, T. N. Mandal, W. S. Yang, Y. H. Lee, S. H. Im, J. H. Noh, S. I. Seok, *Angew. Chem., Int. Ed.* **2014**, 53, 1329.
- [22] X. Liu, J. Chen, M. Luo, M. Leng, Z. Xia, Y. Zhou, S. Qin, D. J. Xue, L. Lv, H. Huang, D. Niu, J. Tang, *ACS Appl. Mater. Interfaces* **2014**, 6, 10687.
- [23] Y. Zhou, L. Wang, S. Chen, S. Qin, X. Liu, J. Chen, D. J. Xue, M. Luo, Y. Cao, Y. Cheng, E. H. Sargent, J. Tang, *Nat. Photonics* **2015**, 9, 409.

- [24] K. Zeng, D. J. Xue, J. Tang, *Semicond. Sci. Technol.* **2016**, *31*, 063001.
- [25] C. Chen, D. C. Bobela, Y. Yang, S. Lu, K. Zeng, C. Ge, B. Yang, L. Gao, Y. Zhao, M. C. Beard, J. Tang, *Front. Optoelectron.* **2017**, *10*, 18.
- [26] B. R. Ramirez, P. K. Nair, *Phys. Status Solidi A* **2018**, *215*, 1800479.
- [27] Z. Li, X. Liang, G. Li, H. Liu, H. Zhang, J. Guo, J. Chen, K. Shen, X. San, W. Yu, R. E. I. Schropp, Y. Mai, *Nat. Commun.* **2019**, *10*, 125.
- [28] Y. Cao, X. Zhu, J. Jiang, C. Liu, J. Zhou, J. Ni, J. Zhang, J. Pang, *Sol. Energy Mater. Sol. Cells* **2020**, *206*, 110279.
- [29] A. Mavlonov, T. Razikov, F. Raziq, J. Gan, J. Chantana, Y. Kawano, T. Nishimura, H. Wei, A. Zakutayev, T. Minemoto, X. Zu, S. Li, L. Qiao, *Sol. Energy* **2020**, *201*, 227.
- [30] J. Zhou, X. Zhang, H. Chen, Z. Tang, D. Meng, K. Chi, Y. Cai, G. Song, Y. Cao, Z. Hu, *Appl. Surface Sci.* **2020**, *534*, 147632.
- [31] T. T. Ngo, S. Chavhan, I. Kosta, O. Miguel, H. J. Grande, R. N. Tena-Zaera, *ACS Appl. Mater. Interfaces* **2014**, *6*, 2836.
- [32] M. Luo, M. Leng, X. Liu, J. Chen, C. Chen, S. Qin, J. Tang, *Appl. Phys. Lett.* **2014**, *104*, 173904.
- [33] M. Leng, M. Luo, C. Chen, S. Qin, J. Chen, J. Zhong, J. Tang, *Appl. Phys. Lett.* **2014**, *105*, 083905.
- [34] C. Chen, L. Wang, L. Gao, D. Nam, D. Li, K. Li, Y. Zhao, C. Ge, H. Cheong, H. Liu, *ACS Energy Lett.* **2017**, *2*, 2125.
- [35] X. Wen, C. Chen, S. Lu, K. Li, R. Kondrotas, Y. Zhao, W. Chen, L. Gao, C. Wang, J. Zhang, G. Niu, J. Tang, *Nat. Commun.* **2018**, *9*, 2179.
- [36] G. X. Liang, Z. H. Zheng, P. Fan, J. T. Luo, J. G. Hu, X. H. Zhang, H. L. Ma, B. Fan, Z. K. Luo, D. P. Zhang, *Sol. Energy Mater. Sol. Cells* **2018**, *174*, 263.
- [37] K. Li, S. Wang, C. Chen, R. Kondrotas, M. Hu, S. Lu, C. Wang, W. Chen, J. Tang, *J. Mater. Chem. A* **2019**, *7*, 9665.
- [38] R. Tang, Z. H. Zheng, Z. H. Su, X. J. Li, Y. D. Wei, X. H. Zhang, Y. Q. Fu, J. T. Luo, P. Fan, G. X. Liang, *Nano Energy* **2019**, *64*, 103929.
- [39] Y. D. Luo, R. Tang, S. Chen, J. G. Hu, Y. K. Liu, Y. F. Li, X. S. Liu, Z. H. Zheng, Z. H. Su, X. F. Ma, P. Fan, X. H. Zhang, H. L. Ma, Z. G. Chen, G. X. Liang, *Chem. Eng. J.* **2020**, *393*, 124599.
- [40] G. X. Liang, Y. D. Luo, S. Chen, R. Tang, Z. H. Zheng, X. J. Li, X. S. Liu, Y. K. Liu, Y. F. Li, X. Y. Chen, Z. H. Su, X. H. Zhang, H. L. Ma, P. Fan, *Nano Energy* **2020**, *73*, 104806.
- [41] L. Lin, L. Jiang, Y. Qiu, B. Fan, *J. Phys. Chem. Solids* **2018**, *122*, 19.
- [42] F. Baig, Y. H. Khattak, B. M. Soucase, S. Beg, S. R. Gillani, S. Ahmed, *J. Nanoelectron. Optoelectron.* **2019**, *14*, 72.
- [43] Y. Cao, X. Zhu, H. Chen, X. Zhang, J. Zhou, Z. Hu, J. Pang, *Sol. Energy Mater. Sol. Cells* **2019**, *200*, 109945.
- [44] F. Baig, Y. H. Khattak, S. Beg, B. M. Soucase, *Optik* **2019**, *197*, 163107.
- [45] Z. Q. Li, M. Ni, X. D. Feng, *Mater. Res. Express* **2020**, *7*, 016416.
- [46] I. Gharibshahian, A. A. Orouji, S. Sharbati, *Sol. Energy Mater. Sol. Cells* **2020**, *212*, 110581.
- [47] F. Baig, Y. H. Khattak, A. Shuja, K. Riaz, B. M. Soucase, *Curr. Appl. Phys.* **2020**, *20*, 973.
- [48] W. Shockley, H. J. Queisser, *J. Appl. Phys.* **1961**, *32*, 510.
- [49] S. Ruhle, *Sol. Energy* **2016**, *130*, 139.
- [50] S. R. A. Ahmed, A. Sunny, S. Rahman, *Sol. Energy Mater. Sol. Cells* **2020**, *221*, 110919.
- [51] P. K. Kung, M. H. Li, P. Y. Lin, Y. H. Chiang, C. R. Chan, T. F. Guo, P. Chen, *Adv. Mater. Interfaces* **2018**, *5*, 1800882.
- [52] Y. Xiao, H. Wang, H. Kuang, *Opt. Mater.* **2020**, *108*, 110414.
- [53] X. Guo, H. J. Xie, J. W. Zheng, H. Xu, Q. Kun, Q.-K. Wang, Y. Q. Li, S. T. Lee, J. X. Tang, *Nanoscale* **2015**, *7*, 867.
- [54] F. Baig, Y. H. Khattak, B. M. Soucase, A. Shehzad, S. Beg, S. Ullah, *Mater. Focus* **2018**, *7*, 777.
- [55] Y. Li, Z. Wang, D. Ren, Y. Liu, A. Zheng, S. M. Zakeeruddin, X. Dong, A. Hagfeldt, M. Grätzel, P. Wang, *ACS Appl. Energy Mater.* **2019**, *2*, 3822.
- [56] W. Albers, C. Haas, H. J. Vink, J. D. Wasscher, *J. Appl. Phys.* **1961**, *32*, 2220.
- [57] P. Sinsermsuksakul, J. Heo, W. Noh, A. S. Hock, R. G. Gordon, *Adv. Energy Mater.* **2011**, *1*, 201100330.
- [58] Y. Kawano, J. Chantana, T. Minemoto, *Curr. Appl. Phys.* **2015**, *15*, 897.
- [59] M. Minbashi, A. Ghobadi, M. H. Eshani, H. R. Dizaji, N. Memarian, *Sol. Energy* **2018**, *176*, 520.
- [60] M. Burgelman, K. Decock, A. Niemegeers, J. Verschraegen, S. Degrave, *SCAPS Manual (version: 3.3.07)*, Department of Electronics and Information Systems, University of Gent, Belgium.
- [61] M. Burgelman, P. Nollet, S. Degrave, *Thin Solid Films* **2000**, *361*, 527.
- [62] M. Burgelman, J. Verschraegen, S. Degrave, P. Nollet, *Prog. Photovolt. Res. Appl.* **2004**, *14*, 143.
- [63] M. Mostefaoui, H. Mazari, S. Khelifi, A. Bouraiou, R. Dabou, *Energy Proc.* **2015**, *74*, 736.
- [64] H. B. Michaelson, *J. Appl. Phys.* **1977**, *48*, 4729.
- [65] S. Dabbabi, T. B. Nasr, N. T. Kamoun, *JOM* **2019**, *71*, 602.
- [66] H. Heriche, Z. Rouabah, N. Bouarissa, *Int. J. Hydrogen Energy* **2017**, *42*, 9524.
- [67] S. O. Oyedele, B. M. Soucase, B. Aka, *IOSRJ. Appl. Phys.* **2016**, *8*, 01.
- [68] O. Madelung, *Semiconductors: Data Handbook*, 3rd ed., Springer, New York **2004**, p. 623.
- [69] M. M. A. Moon, M. H. Ali, M. F. Rahman, A. Kuddus, J. Hossain, A. B. M. Ismail, *Phys. Scr.* **2020**, *95*, 035506.
- [70] T. Minemoto, M. Murata, *Sol. Energy Mater. Sol. Cells* **2015**, *133*, 8.
- [71] S. S. Hegde, A. G. Kunjormana, P. Murahari, B. K. Prasad, K. Ramesh, *Surf. Interfaces* **2018**, *10*, 78.
- [72] M. Shaban, A. M. Bayoumi, D. Farouk, M. B. Saleh, T. Yoshitake, *Solid-State Electron.* **2016**, *123*, 111.
- [73] M. M. A. Moon, M. H. Ali, M. F. Rahman, J. Hossain, A. B. M. Ismail, *Phys. Status Solidi A* **2020**, *217*, 1900921.
- [74] A. Kumar, A. K. Goyal, U. Gupta, Tanya, N. Gupta, R. Chaujar, *Mater. Today: Proc.* **2020**, *28*, 361.
- [75] M. S. Shamna, K. S. Nithya, K. S. Sudheer, *Mater. Today: Proc.* **2020**, *33*, 1246.
- [76] A. Ahmed, K. Riaz, H. Mehmood, T. Tauqeer, Z. Ahmad, *Opt. Mater.* **2020**, *105*, 109897.
- [77] S. M. Sze, K. K. Ng, *Physics of Semiconductor Devices*, 3rd ed., John Wiley & Sons, New York **2007**, pp. 40–43.
- [78] M. K. Omrani, M. Minbashi, N. Memarian, D. H. Kim, *Solid-State Electron.* **2018**, *141*, 50.
- [79] M. D. Wanda, S. Ouédraogo, F. Tchoffo, F. Zougmoré, J. M. B. Ndjaka, *Int. J. Photoenergy* **2016**, *2016*, 2152018.
- [80] C. Chen, K. Li, S. Chen, L. Wang, S. Lu, Y. Liu, D. Li, H. Song, J. Tang, *ACS Energy Lett.* **2018**, *3*, 2335.
- [81] Z. Gu, F. Chen, X. Zhang, Y. Liu, C. Fan, G. Wu, H. Li, H. Chen, *Sol. Energy Mater. Sol. Cells* **2015**, *140*, 396.
- [82] Y. Wang, Z. Xia, J. Liang, X. Wang, Y. Liu, C. Liu, S. Zhang, H. Zhou, *Semicond. Sci. Technol.* **2015**, *30*, 054004.
- [83] J. Tao, X. Hu, J. Xue, Y. Wang, G. Weng, S. Chen, Z. Zhu, J. Chu, *Sol. Energy Mater. Sol. Cells* **2019**, *197*, 1.
- [84] S. G. Kumar, K. S. R. K. Rao, *Energy Environ. Sci.* **2013**, *7*, 45.
- [85] Y. P. Varshni, *Physica* **1967**, *34*, 149.
- [86] P. Singh, N. M. Ravindra, *Sol. Energy Mater. Sol. Cells* **2012**, *101*, 36.
- [87] A. Laidouci, A. Aissat, J. P. Vilcot, *Sol. Energy* **2020**, *211*, 237.
- [88] N. Guirdjebaye, S. Ouédraogo, A. Teyou Ngoupo, G. Mbopda Tcheum, J. Ndjaka, *Opto-Electron. Rev.* **2019**, *27*, 70.
- [89] H. Heriche, Z. Rouabah, N. Bouarissa, *Int. J. Hydrogen Energy* **2017**, *42*, 9524.
- [90] O. Simya, A. Mahaboobbatcha, K. Balachander, *Superlattices Microstruct.* **2015**, *82*, 248.